Research on residual stress inside Fe-Mn-Si shape memory alloy coating by laser cladding processing*

JU Heng (鞠恒), **LIN Cheng-xin** (林成新)**, **ZHANG Jia-qi** (张佳琪), **and LIU Zhi-jie** (刘志杰)
College of Transportation Equipment and Ocean Engineering, Dalian Maritime University, Dalian 116026, China

(Received 5 June 2016)

The stainless Fe-Mn-Si shape memory alloy (SMA) coating was prepared on the surface of AISI 304 stainless steel. The principal residual stress measured by the mechanical hole-drilling method indicates that the Fe-Mn-Si SMA cladding specimen possesses a lower residual stress compared with the 304 stainless steel cladding specimen. The mean stress values of the former and the latter on 10-mm-thick substrate are 4.751 MPa and 7.399 MPa, respectively. What's more, their deformation values on 2-mm-thick substrate are about 0° and 15°, respectively. Meanwhile, the variation trend and the value of the residual stress simulated by the ANSYS finite element software consist with experimental results. The X-ray diffraction (XRD) pattern shows ε-martensite exists in Fe-Mn-Si SMA coating, which verifies the mechanism of low residual stress. That's the γ→ε martensite phase transformation, which relaxes the residual stress of the specimen and reduces its deformation in the laser cladding processing.

Document code: A **Article ID:** 1673-1905(2016)05-0344-5
DOI 10.1007/s11801-016-6131-1

Recently, laser cladding technology draws extensive attention in the aspects of hardening metal matrix composites with ceramic material[1,2]. Contrasted with traditional surface modification, laser cladding coating possesses narrow heat affected zone, refined grain and low dilution rate.

Meanwhile, austenitic stainless steels[3] are extensively used in structural components primarily because of their high resistance to corrosion and oxidation. Thus laser cladding 304 stainless steel coatings can not only offer good prospects of local repair, but also reduce coats in the manufacturing process of plain-carbon-steel components which needs high corrosion resistance surface.

However, due to the expansion in the heat process and the contraction in the cool process, the residual stress generates inside the 304 stainless steel coating[4]. And the stress can lead the deformation of workpiece and the generation of fatigue crack and fatigue break[5]. Presently, the main post-processing method to reduce residual stress includes vibration method[6], ultrasonic method[7], heat treatment method[8], explosion method[9], etc. These methods need additional process and fund, thus it has important significance to develop a low residual stress coating in the laser cladding process.

Because the residual stress generated inside the Fe-Mn-Si shape memory alloy (SMA) coating induces γ→ε martensite phase, which can relax residual stress and reduce deformation. Furthermore, laser cladding is a complicated chemical and physical process, thus difficulties and high cost often accompany with experimental methods. The ANSYS and the ABAQUS finite element softwares are often adopted to numerically simulate[10] the stress field of cladding specimen.

In this paper, stainless Fe-Mn-Si-Cr-Ni SMA coating (test material) and 304 stainless steel coating (contrast material) were prepared on AISI 304 stainless steel surface by a CO_2 laser. The residual stress values of measuring points in cladding specimens were measured by the mechanical hole-drilling method. Meanwhile, the stress field of the cladding model under the same technology condition was simulated by the ANSYS finite element software. And the mechanism which can lead to reduce the residual stress in Fe-Mn-Si-Cr-Ni SMA is demonstrated by X-ray diffraction (XRD)[11].

A DL-LPM-V CO_2 laser with wavelength of 10.6 μm and maximum power of 5 kW was used for the material processing. Because the residual stress is affected with the expansion coefficient, the Fe-Mn-Si-Cr-Ni SMA coating and the 304 stainless steel coating were chosen as experimental material and contrast material for their similar characteristics. These two kinds of laser cladding powder are Fe/Mn/Si/Cr/Ni mixed powder and 304 stainless steel powder (offered by Tianjiu Metallurgy Powder Corporation). The preparation technology of the self-made Fe/Mn/Si/Cr/Ni mixed powder is as follows. (1) Fe, Mn, Si, Cr and Ni element powders were weighed with the mass ratio of 53:32:9:4:2 by analytical balance with measuring accuracy of 0.000 1 mg. (2) The mixed

* This work has been supported by the Fundamental Research Funds for the Central Universities of China (No.3132016354).
** E-mail: lchxin@dlmu.edu.cn

powder was ground by QM-1 horizontal bowl mill for 4 h to obtain the powder which possesses determined chemical component, uniform mixture and fixed particle size of 10—45 μm. (3) The mixed powder was dried by placing it in a DZF-6030B vacuum drying oven at 120 °C for 3 h. And under the process conditions with laser power of 2 kW, laser spot diameter of 3 mm, traverse speed of 800 mm/min, 50% overlap and defocusing amount of +30 mm, 1-mm-thick laser cladding coating was prepared on the surface of two AISI 304 stainless steel substrates whose length, width and height are 100 mm, 50 mm, 10 mm and 100 mm, 30 mm, 2 mm, respectively.

The chemical components of laser cladding coating and substrate were analyzed by QSN750 multi-channel spark direct reading spectrometer, as shown in Tab.1. The chemistry composition of coating is Fe-16Mn-6Si-11Cr-5Ni, belonging to stainless Fe-Mn-Si SMA.

Tab.1 Compositions of AISI 304 stainless steel and Fe-Mn-Si-Cr-Ni SMA coating

Chemistry composition	C	Si	Mn	Ni	Cr	Fe
AISI 304	0.069	0.404	1.148	8.71	18.14	Bal.
Fe-Mn-Si-Cr-Ni SMA	≤0.08	5.89	16.25	4.97	10.98	Bal.

In addition, the residual stress was measured by the hole-drilling method, whose standard was established in 1981 by American Society of Testing Materials (ASTM). The value of the principal residual stress was calculated by substituting the strain values into[12]

$$\begin{cases} \sigma_1 = E(\varepsilon_1+\varepsilon_3)/4A - \\ \quad E\sqrt{(\varepsilon_1-\varepsilon_3)^2+(2\varepsilon_2-\varepsilon_1-\varepsilon_3)^2}/4B \\ \sigma_2 = E(\varepsilon_1+\varepsilon_3)/4A + \\ \quad E\sqrt{(\varepsilon_1-\varepsilon_3)^2+(2\varepsilon_2-\varepsilon_1-\varepsilon_3)^2}/4B \\ \tan 2\theta = (2\varepsilon_2-\varepsilon_1-\varepsilon_3)/(\varepsilon_3-\varepsilon_1) \end{cases}, \quad (1)$$

where ε_1, ε_2 and ε_3 are the strain measured in three directions, σ_1 and σ_2 are the maximum and minimum principal residual stress, θ is the included angle between the direction of σ_1 and the reference axis of No.1 strain gauge, E is the material elasticity modulus, and A, B are the stress release coefficients, which relate to the diameter and depth of drilling hole and the size of strain rosette. The stress release coefficients A and B are -0.276×10^{-12} MPa^{-1} and -0.567×10^{-12} MPa^{-1} which were measured through CB3395-92 standard. Meanwhile, in the test, the bit diameter D_0, the drilling depth h and the distance D between the center of hole drilling and the edge of strain gauge is Φ1.5 mm, 1.8 mm and Φ5 mm, respectively. The strain value was measured by mean value method in which strain value is read each 5 min within 35 min after drilling[13]. The schematic diagram of the specimen is shown Fig.2(a), and the distribution of the measuring points is shown in Fig.2(b). Here, six measuring points are parallel to the laser scanning direction, and are 10 mm away from coating's lower edge. The 1# measuring point is 12.5 mm away from substrate's left margin, and the interval between adjacent points is 15 mm.

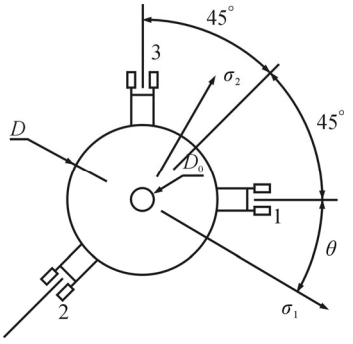

Fig.1 Arrangement of the strain gauge

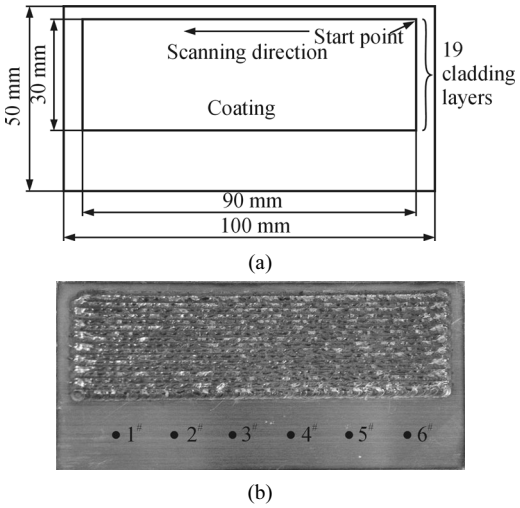

Fig.2 (a) Schematic diagram of specimen; (b) Distribution of measuring points

The strain ε_1, ε_2, ε_3 and the maximum principal residual stress σ_1 of measuring points in Fe-Mn-Si-Cr-Ni laser cladding specimen and the 304 stainless steel are shown in Tabs.2 and 3.

Tab.2 The strain ε_1, ε_2, ε_3 and the maximum principal residual stress σ_1 of measuring points in the Fe-Mn-Si-Cr-Ni SMA cladding specimen

Number	ε_1 ($\times10^{-6}$)	ε_2 ($\times10^{-6}$)	ε_3 ($\times10^{-6}$)	σ_1 (MPa)
1#	33.594	−26.187	−25.428	6.006
2#	28.888	−25.913	−22.102	5.650
3#	49.388	−13.174	−19.121	2.366
4#	28.936	−4.748	−44.337	4.046
5#	14.452	9.873	−20.625	4.898
6#	29.609	7.886	−29.987	5.541

Tab.3 The strain ε_1, ε_2, ε_3 and the maximum principal residual stress σ_1 of measuring points in the 304 stainless steel cladding specimen

Number	ε_1 ($\times10^{-6}$)	ε_2 ($\times10^{-6}$)	ε_3 ($\times10^{-6}$)	σ_1 (MPa)
1#	74.653	−18.390	−45.307	6.797
2#	80.532	−25.497	−47.441	7.546
3#	58.764	−20.951	−35.700	5.951
4#	48.477	−4.764	−40.596	6.772
5#	38.076	9.361	−41.104	7.828
6#	7.969	30.249	−21.419	9.501

Under the same technological condition, the principal residual stress values of the Fe-Mn-Si-Cr-Ni SMA specimen and the 304 stainless steel specimen obtained from Tabs.2 and 3 are shown in Fig.3. It is obvious that the principal residual stress of Fe-Mn-Si-Cr-Ni SMA cladding specimen is less than that of 304 stainless steel cladding specimen in corresponding positions. The mean principal residual stress values of 1#~6# measuring points in Fe-Mn-Si-Cr-Ni SMA coating and 304 stainless steel coating are 4.751 MPa and 7.399 MPa, respectively. The former is 35.7% lower than the latter.

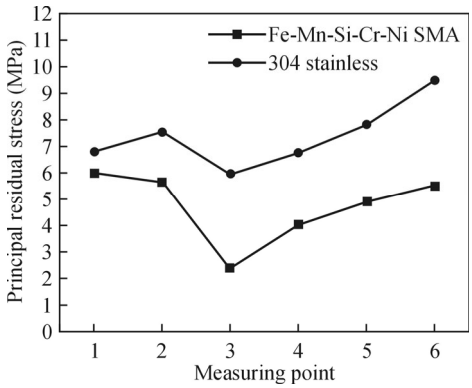

Fig.3 Principal residual stress values of measuring points in Fe-Mn-Si-Cr-Ni SMA specimen and 304 stainless steel specimen

The variation trends of the residual stress in two cladding specimens are consistent. When the laser spot irradiates the coating, it preheats the zone which hasn't been cladded. In addition, the laser heat source is like a heat treatment for the processed zone after the laser cladding. And the time of preheating and heat treating in two sides is lower than that in the middle region, thus the temperature gradient of the former is higher than that of the latter. It is well known that the residual stress is directly proportional to the temperature gradient. Consequently, the residual stress of the middle region is lower than those of the two sides.

The deformations of the 304 stainless steel coating specimen and the Fe-Mn-Si-Cr-Ni SMA coating specimen cladded on 2-mm-thick AISI 304 stainless steel sheet are shown in Fig.4. From Fig.4, it is indicated that the deformation angles between the edge of cladding specimens and the horizontal direction are about 15° and 0°, respectively. That also concludes that the Fe-Mn-Si-Cr-Ni cladded specimen possesses a lower residual stress.

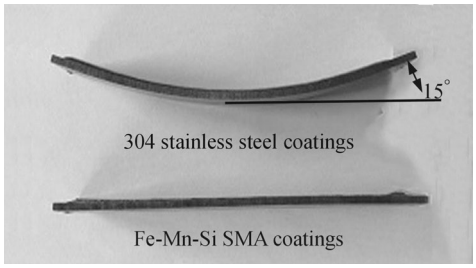

Fig.4 Deformations of 304 stainless steel and Fe-Mn-Si-Cr-Ni SMA cladding coating samples

The temperature and stress fields of the cladded specimens were numerical simulated by ANSYS finite element software. Some settings of the simulation are as follow.

According to the geometry size of cladding specimen shown in Fig.2, three-dimensional finite element model is established. The unit of cladding material and the substrate is SOLID90 and SOLID70, respectively. And meshing unit size is increased with the increase of its distance away from the coating to assure the computation precision and save the calculation time.

Tabs.4 and 5 show the material properties (parameters defined for the temperature field and stress field) of Fe-Mn-Si-Cr-Ni SMA coating and AISI 304 stainless steel, which are taken from Refs.[14]—[16] and JMatpro software.

Tab.4 Properties of the Fe-Mn-Si-Cr-Ni SMA coating

Temperature(°C)	20	100	300	500	800	1 200	1 300	1 450	1 800
Density (kg/m^3)	7 870	7 493	7 383	7 271	7 069	6 761	6 483	6 389	6 031
Thermal conductivity (W·m^{-1}·K^{-1})	14.7	15.7	18.5	21.3	25.0	28.9	27.8	30.0	35.4
Specific heat (J·kg^{-1}·K^{-1})	495	502	539	575	757	703	4 672	812	848
Coefficient of thermal expansion (10^{-5} K^{-1})	2.37	2.40	2.47	2.53	2.82	3.24	4.24	4.46	5.68
Enthalpy (J·g^{-1})	−154	−117	−13	98	295	617	858	1 012	1 306
Elastic modulus ($\times10^{10}$ Pa)	17.89	17.39	16.00	14.51	11.86	7.992	0.046	0	0
Poisson ration	0.296	0.299	0.306	0.314	0.325	0.341	0.476	0.5	0.5
Yield strength ($\times10^8$ Pa)	6.37	5.70	5.12	4.08	2.03	0.12	0.01	0	0
Shear modula ($\times10^9$ Pa)	69.00	66.93	61.21	55.20	44.74	29.79	0.015	0	0

Tab.5 Properties of the AISI 304 stainless steel

Temperature (°C)	20	200	400	600	800	1 000	1 400	1 454	1 800
Density (kg/m^3)	8 020	7 950	7 860	7 750	7 645	7 530	7 300	6 900	6 615
Thermal conductivity (W·m^{-1}·K^{-1})	14.85	18.41	22.41	26.41	30.41	34.41	42.41	36.54	50.41
Specific heat (J·kg^{-1}·K^{-1})	449	502	562	1026	617	634	919	5 011	839
Coefficient of thermal expansion (10^{-5} K^{-1})	16.5	17.7	18.3	19.0	19.7	—	20.8	—	21.0
Enthalpy (J·g^{-1})	107	191	297	418	559	687	973	1 106	1 480
Elastic modulus ($\times10^{10}$ Pa)	20.5	19.5	17.8	15.9	13.6	11.8	7.49	0.42	0
Poisson ration	0.295	0.308	0.320	0.335	0.345	0.365	0.375	0.45	0.45
Yield strength ($\times10^8$ Pa)	1.80	1.30	1.08	0.82	0.69	—	0.63	0.60	0
Ultimate tensile strength ($\times10^8$ Pa)	5.86	4.96	4.39	3.50	2.00	0.57	0.54	0.50	0

The ANSYS APDL programming language and life-death element technique are adopted to simulate the metallurgical bonding between the powder and the substrate with moving the simulation source (Gauss heat source).

The temperature units in the temperature field are converted into structure units for the simulation of stress field, and the temperature field result is applied as the load for the stress field analysis.

The boundary condition of stress field includes the displacement constraints in *X*, *Y* and *Z* directions which are applied on three vertices of the substrate and the lower surface of coating to limit the rigid displacement of model and to avoid stress concentration. The mesh generation and constraint form are shown in Fig.5.

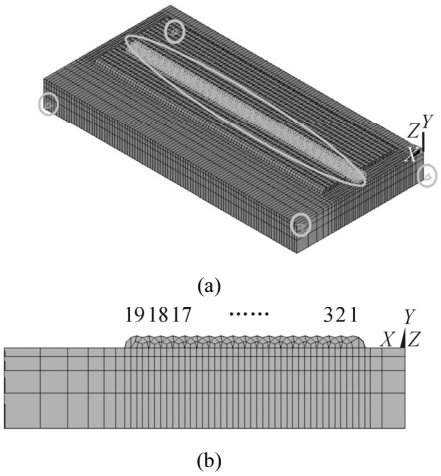

Fig.5 (a) Displacement constraint and (b) mesh generation of the finite element model

The principal residual stress of each point measured by hole-drilling method in Fe-Mn-Si-Cr-Ni SMA cladding specimen and the major principal strain curve simulated by ANSYS finite element software in the path which parallels to laser scanning direction and uses 1# and 6# measuring points as two endpoints are shown in Fig.6.

Although the variation tends of residual stress in numerical simulation and experimental test are consistent, the error still exists between them. One of the reasons is that the Gauss heat source is an ideal heat source, while the actual laser heat source distributes unequally which is influenced by material surface state and internal material components. Other one is that mesh size can't absolutely match the powder.

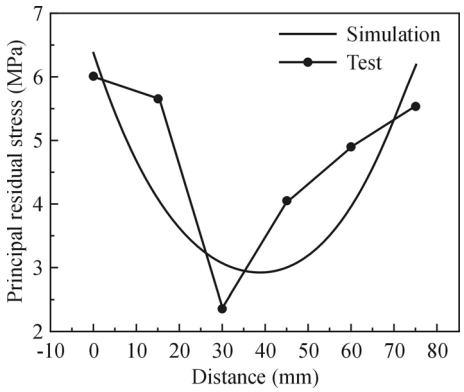

Fig.6 Residual principal stress value σ_1 in the test and simulation along the path paralleling to laser scanning direction

The results of experiment and simulation clearly show that Fe-Mn-Si-Cr-Ni SMA coating possesses low residual stress. The mechanism is inferred that the residual stress of Fe-Mn-Si-Cr-Ni SMA coating as the phase transition drives force to induce γ→ε martensite phase transformation[17], and the phase transformation relaxes the residual stress of the cladding layer.

The phase composition of Fe-Mn-Si-Cr-Ni cladding coating was analyzed by X-ray diffractometer to verify the above analysis. The XRD patterns of Fe-Mn-Si-Cr-Ni SMA coating before and after solid solution (1 000 °C, 1 h)are shown as Fig.7.

As shown in Fig.7, γ austenite and ε martensite exist in Fe-Mn-Si-Cr-Ni cladding coating before solid solution, and only γ austenite exists after solid solution. It is indicated that γ→ε martensite phase transformation occurs on Fe-Mn-Si-Cr-Ni SMA coating in the laser cladding process, and residual stress of laser cladding coating is

the driving force of the phase transformation.

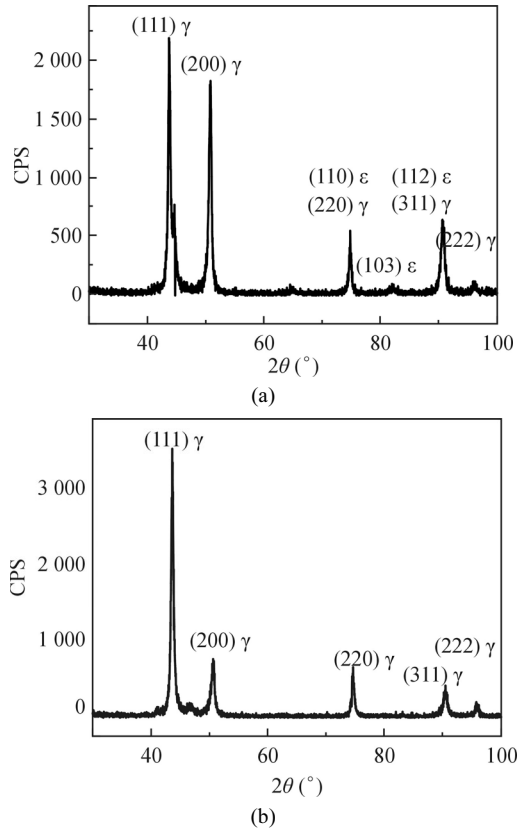

Fig.7 XRD patterns of the Fe-Mn-Si-Cr-Ni coating (a) before and (b) after solid solution

Fe-Mn-Si-Cr-Ni SMA coating was in-situ prepared by laser cladding process. The variation tends of residual stress obtained in simulation and experiment are consistent. The mean stress values of Fe-Mn-Si-Cr-Ni SMA cladding specimen and 304 stainless steel cladding specimen at measuring points in the 10-mm-thick substrate are 4.751 MPa and 7.399 MPa, and their deformation angles on 2-mm-thick substrate are about 0° and 15°, respectively. The residual stress in cladding coating induces γ→ε martensite phase transformation in the laser cladding process of in-situ synthesis of Fe-Mn-Si SMA coating, and the phase transformation relaxes stress and reduces specimens' deformation.

References

[1] ZHANG Hui, ZOU Yong, ZOU Zeng-da and WU Dong-ting, Optics & Laser Technology **65**, 119 (2015).

[2] Tomaž Kek and Janez Grum, Journal of Mechanical Engineering **56**, 150 (2010).

[3] Guo Hong, LIANG Cheng, HUA Xiu-chun, MA Hai-sheng, GUO Wen-feng, JING Cheng-Bin and CHU Jun-hao, Journal of Optoelectronics·Laser **26**, 393 (2015). (in Chinese)

[4] S. W. Dean, Zoran Bergant, Slabe Janez Marko, Ocana Jose Luis and Janez Grum, Journal of ASTM International **8**, 2 (2001).

[5] CHAO Zeng, WEI Tian, LIAO Wen-he and LIANG Hua, Surface and Coatings Technology **236**, 309 (2013).

[6] Wang Jia-siang, Hsieh Chih-chun, Lai Hsuan-han, Kuo Che-wei, Wu Paxon Ti-yuan and Wu Weite, Materials Characterization **99**, 248 (2015).

[7] Shalvand M., Hojjat Y., Abdullah A. and Asadi H., Materials & Design **33**, 713 (2013).

[8] Panchal Vikas D., World Pumps **2013**, 28 (2013).

[9] Zhang J., Liu K., Zhao K., Li X., Liu Y. and Zhang K., International Journal of Solids and Structures **42**, 3784 (2005).

[10] ZANG Yan-nan and NI Xiao-wu, Journal of Optoelectronics·Laser **26**, 1835 (2015). (in Chinese)

[11] WU Dong-ni, CUI Rui-rui and DENG Chao-yong, Journal of Optoelectronics·Laser **25**, 1516 (2014). (in Chinese)

[12] S. Sánchez-Beitia, M. Crespo de Antonio and L. Acuna, Construction & Building Materials **93**, 798 (2015).

[13] YANG Jian, CHEN Jing, YANG Hai-ou, LIN Xin and HUANG Wei-dong, Rare Metal Materials and Engineering **33**, 1305 (2004). (in Chinese)

[14] WANG Ren-ping, LEI Yong-ping and SHI Yao-wu, Optics & Laser Technology **43**, 870 (2010).

[15] YANG Qing-xiang, ZHANG Yun-kun, ZHANG Yue, FANG Yuan, LIAO Biao and YAO Mei, Transactions of Materials and Heat Treatment **320**, 183 (2009). (in Chinese)

[16] ZHOU Chou-yu, Lin CHENG-xin, GUAN Hui-feng and SUN De-ping, Journal of Dalian Maritime University **4**, 75 (2014). (in Chinese)

[17] XU Zhu-yao, Shape Memory Materials, Shanghai: Shanghai Jiao Tong University Press. (in Chinese)